Icarus **154**, 372–380 (2001)
doi:10.1006/icar.2001.6711, available online at http://www.idealibrary.com on IDEAL®

# Carbon Suboxide in Astrophysical Ice Analogs

P. A. Gerakines[1] and M. H. Moore

*Astrochemistry Branch, Code 691, NASA's Goddard Space Flight Center, Greenbelt, Maryland 20771*
E-mail: gerakines@uab.edu

Received January 18, 2001; revised July 5, 2001

**As suggested by W. T. Huntress *et al.* (1991, *Nature* 352, 316–318), carbon suboxide ($C_3O_2$) is a potential extended source of both the CO and atomic carbon emission observed in cometary comae. However, laboratory experiments on the formation and stability of $C_3O_2$ in space environments have not been published. In this work, we study solid $C_3O_2$ in ices representative of cometary nuclei as well as interstellar icy grain mantles, specifically addressing the issues of $C_3O_2$ formation and stability under exposure to energetic processing in the forms of proton irradiation and UV photolysis. The formation rate of $C_3O_2$ is measured in laboratory ices of pure CO and $CO_2$ and mixtures of these molecules with $H_2O$ at 18 K. Destruction rates in $H_2O$-dominated mixtures appropriate to a cometary nucleus or interstellar icy grain mantle are also measured. Differences in rates between photolysis and irradiation experiments are observed and quantified. Mid-infrared spectra of $C_3O_2$-containing mixtures are presented together with measurements of carbon suboxide's infrared band strengths and vapor pressures from 110 to 125 K. Implications are discussed for the existence of $C_3O_2$ under the energetic conditions found in astrophysical environments as well as the possibility for its detection in cometary and/or interstellar ices.** 

*Key Words:* **ices; comets, composition; radiation chemistry; photochemistry; spectroscopy.**

## 1. INTRODUCTION

Huntress *et al.* (1991) proposed carbon suboxide ($C_3O_2$) as a possible source of both the extended neutral atomic carbon and molecular carbon monoxide emission observed in the coma of Comet Halley (e.g., Festou *et al.* 1986, Woods *et al.* 1987, Eberhardt *et al.* 1987). $C_3O_2$ is a well-studied oxide of carbon, made up of two carbon monoxide groups linked to a carbon atom to form a linear structure: O=C=C=C=O. In the laboratory, it is widely used as a source of atomic carbon. As a gas it can be stored in a bulb at a pressure of a few mm Hg, but under conditions of standard temperature and pressure (300 K, 1 atm), $C_3O_2$ forms a yellow, red, or brown polymer. (The yellowish clouds on Venus were once attributed to $C_3O_2$ polymer by Kuiper (1957), but Plummer and Carson (1970) later presented spectroscopic evidence proving this to be incorrect.) Suboxide polymers form when CO is processed (by electrolysis, irradiation, or photolysis) in the gas, liquid, or condensed phase (e.g., Lind 1928, Sugimoto *et al.* 1986, Briggs and Clay 1968, Haring *et al.* 1984). Studies of the electrical discharge of CO date back to Brodie (1873) who first showed that its decomposition products formed a reddish brown solid. If present on the surfaces of cometary nuclei, $C_3O_2$ polymers may contribute to their low geometric albedo, which is typically around 4% (as measured toward Comet Halley by, e.g., Sagdeev *et al.* (1986)).

Spectral features of monomeric $C_3O_2$ are unobservable in the gas phase of the interstellar medium or in cometary comae, because $C_3O_2$ is a linear, symmetric molecule with no dipole moment and hence no rotational transitions at submillimeter or radio wavelengths. It may be possible to detect cosmic $C_3O_2$ in the solid phase, however, since it forms a highly interactive crystalline matrix with a variety of absorption features throughout the mid-infrared region, e.g., Miller and Fateley (1964).

In this paper, we study $C_3O_2$ under conditions that more appropriately reflect the environments and compositions of cometary and interstellar ices in order to understand its formation and stability in an astrophysical context. Experimental results are presented for solid $C_3O_2$ formation and energetic processing in laboratory analogs of astrophysical ices (both cometary and interstellar) at low temperature, $T = 15$–$20$ K. The laboratory system, sample preparation, and processing techniques are described in Section 2. Mid-IR spectra (5000–400 $cm^{-1}$; 2–25 $\mu$m) for $C_3O_2$ diluted in different ice matrices at 18 K are presented in Section 3, along with calculations of the strengths ("*A* values") of the $C_3O_2$ IR absorption features and $C_3O_2$ vapor pressures from 110 to 125 K. The formation of $C_3O_2$ resulting from energetic processing of CO and $CO_2$ in pure form and in mixtures with $H_2O$ by both proton irradiation and UV photolysis[2] is measured in Section 4, together with destruction rates in $H_2O$-dominated matrices. Implications for the existence of $C_3O_2$ in

[1] Current address: Astro- and Solar-System Physics Program, Department of Physics, University of Alabama at Birmingham, 1300 University Boulevard, Birmingham, AL 35294-1170.

[2] Hereafter, to clearly distinguish one from the other, we refer to energetic processing by high-energy particles such as protons as "irradiation" and to processing by ultraviolet light as "photolysis."



0019-1035/01 $35.00

the ices found within interstellar clouds and in cometary nuclei and the possibilities for its detection in those environments are discussed in Section 5.

## 2. EXPERIMENTAL

Hudson and Moore (1995) have described the laboratory setup at NASA's Goddard Space Flight Center in detail. In summary, gases are prepared inside a vacuum manifold and vapor-condensed onto a cold (15–20 K) aluminum mirror suspended inside a stainless-steel high-vacuum chamber ($P \approx 10^{-7}$ mm Hg). Mixing ratios in the resultant ice are determined from the partial pressures inside the gas-filled manifold before condensation. Actual ratios in the resulting ice samples may vary slightly from these values because of effects of depositing through a narrow tube, (see, e.g., the discussion in Gerakines *et al.* (1995)), but any differences should not exceed a factor of 2. Since the differences in mixing ratios between the ice mixtures studied are large (100 : 1 or 10 : 1 matrix : suboxide ices are compared to those with ratios of about 1 : 1), the qualitative differences between the 100 : 1 or 10 : 1 ices and the 1 : 1 ices should not be significantly affected (such as those observed in the IR spectra; see Section 3). The quantitative measurements made do not depend critically upon the mixing ratio, but on the general nature of the ice (such as the rates of $C_3O_2$ formation in various pure ices and in an $H_2O$-dominated ice; see Section 3).

The temperature of the mirror may be controlled up to room temperature. IR spectra (with a spectral range of 5000 to 400 $cm^{-1}$ and resolutions from 1 to 4 $cm^{-1}$) are taken by diverting the beam of an FTIR spectrometer (Mattson Instruments) toward the ice-covered mirror, where it passes through the ice before and after reflection at the ice–mirror interface. Ices are processed by turning the mirror to face either a beam of 0.8-MeV protons generated by a Van de Graaff accelerator or UV photons from a microwave-discharged hydrogen flow lamp. Photons from the UV lamp, limited by the LiF window between the $H_2$ discharge and the vacuum system, fall in the wavelength range of 110–250 nm. The total UV photon flux at the ice sample was determined to be approximately $8.6 \times 10^{13}$ photons $cm^{-2}$ $s^{-1}$ by Gerakines *et al.* (2000), who describe this measurement in detail and outline the methods by which both irradiation and photolysis energy doses are calculated.

The $C_3O_2$ used in these experiments was generated by the method described by Miller and Fateley (1964). In summary, a mixture of $CH_2(COOH)_2$ (malonic acid) and $P_2O_5$ (phosphorus pentoxide) in approximate 10 : 1 weight ratio was heated to 410–420 K for 1 h. The gases produced ($H_2O$, $CO_2$, $C_3O_2$, and $CH_3COOH$) were collected at 77 K using liquid $N_2$. The $CO_2$ was removed from the sample by replacing the liquid $N_2$ with a liquid–solid bath of ethanol at 156 K and pumping on the sample for 1 h. To remove the $C_3O_2$ from the remaining sample, the ethanol was replaced by a liquid–solid chloroform ($CHCl_3$) bath at 210 K and the evaporated $C_3O_2$ transferred to a bulb cooled with liquid $N_2$. We produced about 5 torr-liters of $C_3O_2$ (0.3 mmol) from approximately 5 g (50 mmol) of malonic acid using this method. Over the course of several days, the $C_3O_2$ stored in the glass bulb at about 15 torr was seen to decompose (through spectroscopy of the contents of the gas bulb) into $CO_2$ (approximately 1 torr of $CO_2$ per week of storage). This $CO_2$ gas was removed before each experiment using a liquid–solid bath of ethanol as described above.

Reagents used and their purities are as follows: $H_2O$ (triply distilled, with a resistance greater than $10^7$ ohm cm), CO (gas, Matheson, 99.99%), $CO_2$ (gas, Matheson, 99.995%), $N_2$ (gas, Air Products, 99.9995%), malonic acid, $CH_2(COOH)_2$ (Aldrich, 99% purity), and phosphorous pentoxide, $P_2O_5$ (Aldrich, 98% purity).

## 3. RESULTS

### *Infrared Spectral Properties*

The mid-IR spectrum (5000–400 $cm^{-1}$ or 2–25 $\mu$m) of pure $C_3O_2$ at 18 K is shown in Fig. 1 at a resolution of 4 $cm^{-1}$. Peak positions and vibrational mode assignments are listed in Table I. They are in close agreement with those of pure $C_3O_2$ at 100 K reported by Miller and Fateley (1964) and matrix-isolated $C_3O_2$ in Ar (Ames *et al.* 1963, Miller and Fateley 1964, Smith and Leroi 1966).

The strongest absorption in the IR spectrum of $C_3O_2$ (Fig. 1) is its $\nu_3$ anti-symmetric stretching vibration that falls near 2200 $cm^{-1}$ (4.5 $\mu$m). Using standard methods (of condensing a sample to a known thickness and assuming a mass density of 1 g $cm^{-3}$), we used the area under this feature to calculate its integrated absorbance (a.k.a. "band strength" or "$A$ value") of $A(C_3O_2, \nu_3) = (1.3 \pm 0.2) \times 10^{-16}$ cm $molecule^{-1}$. (Since we have assumed a mass density equal to that of water in our

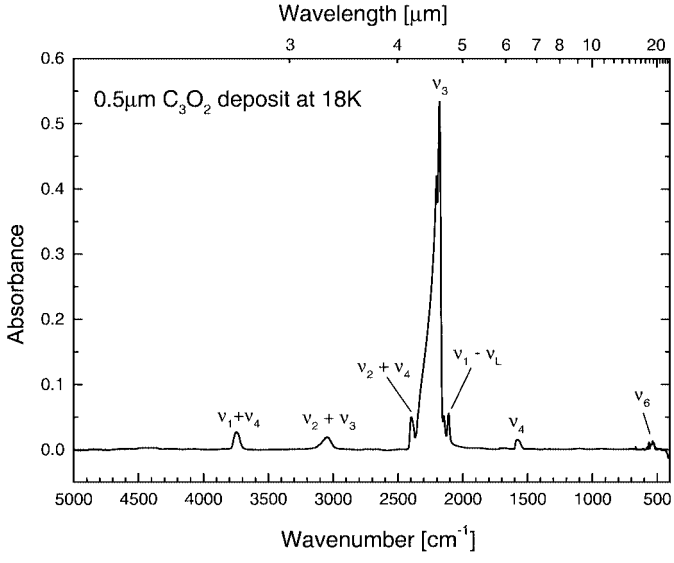


**FIG. 1.** Mid-IR spectrum (5000–400 $cm^{-1}$, 2–25 $\mu$m) of pure $C_3O_2$ at 18 K. Band assignments are taken from Miller and Fateley (1964) and Smith and Leroi (1966).

**TABLE I**
**Observed Mid-IR Spectrum of Pure $C_3O_2$ at 18 K**

| Position ($cm^{-1}$) | Assignment[a] | Band strength, $A$ ($10^{-18}$ cm molecule$^{-1}$) | Comment |
|---|---|---|---|
| 3744 m | $\nu_1 + \nu_4$ | $3.8 \pm 0.6$ | |
| 3043 m | $\nu_2 + \nu_3$ | $6 \pm 1$ | |
| 2756 vw | $\nu_1 + \nu_6$ | — | |
| 2666 vw | $\nu_4 + \nu_5$ | — | |
| 2396 m | $\nu_2 + \nu_4$ | $8 \pm 4$ | |
| 2200, 2177 vs | $\nu_3$ | $130 \pm 20$ | CCO asym. str |
| 2109 m | $\nu_1 - \nu_L$ | — | |
| 1581 m | $\nu_4$ | $5 \pm 3$ | CC asym. str |
| ~540 w | $\nu_6$ | $1.4 \pm 0.3$ | bend |

[a] Assignments taken from Miller and Fateley (1964) and Smith and Leroi (1966).

calculations, the "true" magnitude of $A$ will scale inversely with the actual mass density of the $C_3O_2$ ice sample, which is unknown. The precision of our measurement is unaffected by the value of mass density.) This value of $A$ is about 15–20 times stronger than any of the other observed $C_3O_2$ mid-IR features (see Table I). It is comparable to that of the $\nu_3$ stretching vibration of $H_2O$ at 3240 $cm^{-1}$ (3.1 $\mu$m), which has a band strength of about $1.6 \times 10^{-16}$ cm molecule$^{-1}$ (Hagen *et al.* 1983). The strength of the stretching vibration of CO near 2140 $cm^{-1}$ (4.67 $\mu$m) is 10 times lower than that of $C_3O_2$, at $1.1 \times 10^{-17}$ cm molecule$^{-1}$ (Jiang *et al.* 1975).

Pure $C_3O_2$ sublimes during warming in our system near 120 K. Evidence for a possible phase change (based upon changes in two of the overtone features) is seen between 50 and 75 K. McDougall and Kilpatrick (1965), who measured various thermodynamic properties of $C_3O_2$ over this temperature range, did not find evidence for a solid–solid phase transition, but the IR spectroscopic data (Fig. 2) do suggest a structural change in the $C_3O_2$ ice. Figure 2 contains spectra of the $\nu_1 + \nu_4$ (4000–3500 $cm^{-1}$), $\nu_3$ (2500–2000 $cm^{-1}$), and $\nu_4$ (1700–1450 $cm^{-1}$) $C_3O_2$ absorption features at 22, 50, 75, and 100 K. A gradual change is apparent in the $\nu_1 + \nu_4$ and $\nu_4$ features from 50 to 100 K, indicated by shifts in peak position, decreases in width, and increases in peak absorbance. The $\nu_3$ feature itself does not exhibit any significant changes over this temperature range, although the widths and peak absorbance values for its subpeaks near 2400 and 2100 $cm^{-1}$ do show change.

The $C_3O_2$ $\nu_3$ stretching feature's position, width, and profile are all sensitive to the dilution of $C_3O_2$ in an ice matrix. Figure 3 contains the 2500–2000 $cm^{-1}$ (4–5 $\mu$m) spectra of pure $C_3O_2$ (from Fig. 1), and $C_3O_2$ diluted in matrices of $N_2$, $CO_2$, $H_2O$, and CO. Dilution factors are 100 : 1 (matrix : suboxide) except in the $H_2O$-dominated ice, where it is 10 : 1. The $\nu_3$ peak position (marked with asterisks in Fig. 3) varies by more than 50 $cm^{-1}$ as a result of the change in the ice matrix, from 2253 $cm^{-1}$ in an $N_2$ matrix to 2200 $cm^{-1}$ in the pure $C_3O_2$ sample (there is also a subpeak that falls at 2178 $cm^{-1}$ in the pure $C_3O_2$ sample). The width and profile of the feature also vary depending on the

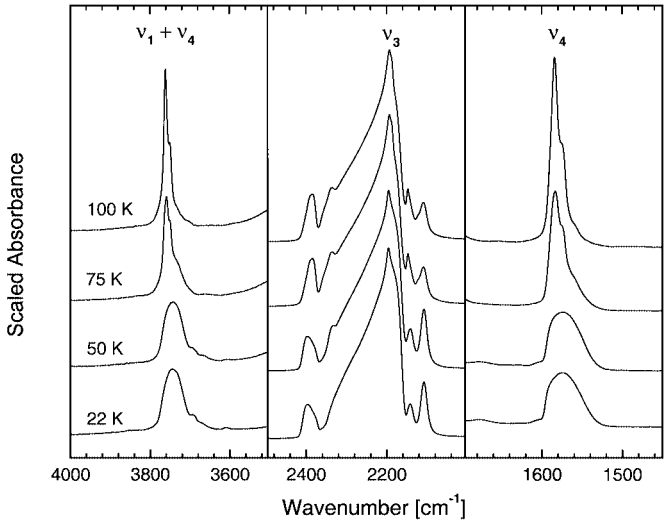


**FIG. 2.** Three features of pure $C_3O_2$: the $\nu_1 + \nu_4$ feature from 4000 to 3500 $cm^{-1}$ (left box), the $\nu_3$ feature from 2500 to 2000 $cm^{-1}$ (middle box), and the $\nu_4$ feature from 1700 to 1450 $cm^{-1}$ (right box) at temperatures of 22, 50, 75, and 100 K (from bottom to top).

matrix. It is sharp and singly peaked in matrices of $N_2$, CO, and $CO_2$ (FWHM = 8–14 $cm^{-1}$). It takes on a broad Gaussian profile when diluted in an $H_2O$ matrix (FWHM = 90 $cm^{-1}$), since the polar nature of the $H_2O$ ice creates a high degree of molecular

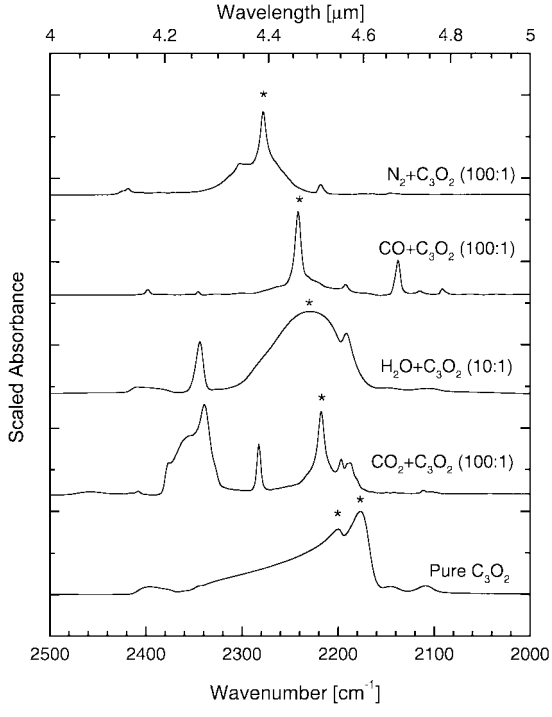


**FIG. 3.** Mid-IR spectra of the $C_3O_2$ $\nu_3$ asymmetric stretching fundamental from 2500 to 2000 $cm^{-1}$ (4 to 5 $\mu$m) for $C_3O_2$ in various ice matrices at 18 K. From top to bottom: $N_2 + C_3O_2$ (100 : 1), $CO + C_3O_2$ (100 : 1), $H_2O + C_3O_2$ (10 : 1), $CO_2 + C_3O_2$ (100 : 1), and pure $C_3O_2$. The peak position of the $\nu_3$ feature is marked with an asterisk in each case.

**TABLE II**
**Position and Width (FWHM) of the $C_3O_2$ $\nu_3$ Stretching Feature in Selected Mixtures at 18 K**

| Ice mixture | Position ($cm^{-1}$) | FWHM ($cm^{-1}$) |
|---|---|---|
| Pure $C_3O_2$ | 2200, 2178 | 67 |
| $CO_2 + C_3O_2$ (100 : 1) | 2217 | 11 |
| $H_2O + C_3O_2$ (10 : 1) | 2233 | 90 |
| $CO + C_3O_2$ (100 : 1) | 2242 | 8 |
| $N_2 + C_3O_2$ (100 : 1) | 2253 | 14 |

interaction. In a pure $C_3O_2$ sample, the stretching feature is broad (FWHM = 67 $cm^{-1}$), double-peaked (peaks falling at 2200 and 2178 $cm^{-1}$), and asymmetric, with a long-wavelength wing that extends to about 2350 $cm^{-1}$ (4.26 $\mu$m). Within the 2200–2300 $cm^{-1}$ region, there is also a notable amount of substructure to the $C_3O_2$ feature, possibly because of $C_3O_2$ dimers, trimers, or higher $n$-mers. Table II summarizes the $\nu_3$ peak's position and FWHM for pure $C_3O_2$ and $C_3O_2$ in several different ice matrices at 18 K.

*Vapor Pressure*

The vapor pressure ($P_{vap}$) of $C_3O_2$ was measured at 110, 115, 120, and 125 K by observing the sublimation rate (d$N$/dt, in $cm^{-2}$ $s^{-1}$) for about 30 minutes at each temperature and using the relation

$$P_{vap} = (\mathrm{d}N/\mathrm{dt}) \times (2\pi\, m\, \mathrm{kT})^{1/2}, \quad (1)$$

where $m$ is the molecular mass of $C_3O_2$ (68 amu). The term d$N$/dt was determined at each temperature of interest by holding the sample at that temperature and measuring the linear change in $N$ versus time. The term $N$ was measured at various time steps by integrating the area underneath the $C_3O_2$ $\nu_3$ feature and dividing by its band strength (the measurement of which is described previously in this section). Calculated values of $P_{vap}$ are listed in Table III. At 110 K, pure $C_3O_2$ has a vapor pressure of $1.2 \times 10^{-8}$ mm Hg, but at 125 K, it has risen sharply to $5.8 \times 10^{-6}$ mm Hg ($C_3O_2$ vapor pressures for $T$ = 160–248 K have been measured by McDougall and Kilpatrick (1965)). In comparison, the vapor pressure of $H_2O$ ice, which depends on its crystalline state, can vary from $\sim 10^{-7}$ to $\sim 10^{-6}$ mm Hg at 125 K (Kouchi 1987).

**TABLE III**
**Vapor Pressure of $C_3O_2$**

| $T$ (K) | $P$ ($10^{-7}$ mm Hg) |
|---|---|
| 110 | $0.12 \pm 0.01$ |
| 115 | $0.90 \pm 0.13$ |
| 120 | $2.1 \pm 0.1$ |
| 125 | $58 \pm 1$ |

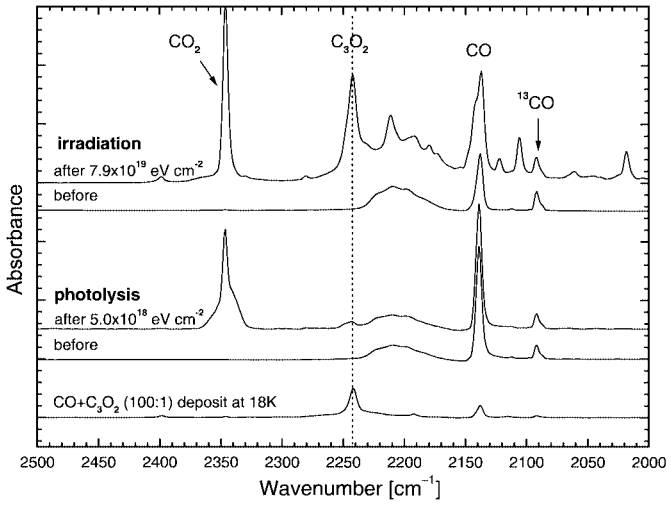


**FIG. 4.** Spectra of pure CO from 2500 to 2000 $cm^{-1}$ (4 to 5 $\mu$m) before and after processing at 18 K by proton irradiation (to a dose of $7.9 \times 10^{19}$ eV $cm^{-2}$) and UV photolysis (to a dose of $5.0 \times 10^{18}$ eV $cm^{-2}$). The spectrum of $CO + C_3O_2$ (100 : 1) at 18 K (bottom) is shown fom comparison. The dotted line indicates the peak position of the $C_3O_2$ stretching feature in the $CO + C_3O_2$ (100 : 1) ice.

*Suboxide Formation and Energetic Processing*

As noted above, $C_3O_2$ and/or $C_3O_2$ polymers are known to form from pure CO energetically processed in its gas (Sugimoto *et al*. 1986), liquid (Briggs and Clay 1968), or solid phases (Haring *et al*. 1984). Here, we measure the production rates of $C_3O_2$ from pure, solid CO at 18 K as processed by irradiation and by photolysis. This is the first direct comparison of pure CO irradiation and photolysis known to us. The IR spectrum of the pure CO sample at 18 K before and after processing is shown in Fig. 4 for each case. The spectrum of the $CO + C_3O_2$ 100 : 1 sample from Fig. 3 is presented for comparison; note that the broad feature near 2210 $cm^{-1}$ present in each of the pure CO spectra is not due to an impurity in the CO ice, but it is a weak absorption of CO itself exaggerated by the scale of the figure and is due to a combination of the CO lattice mode and fundamental stretching mode; see, e.g., Ewing and Pimentel (1961) or Pipes *et al*. (1978) for identifications of this feature. A forest of absorptions appears in the 2500–2000 $cm^{-1}$ (4–5 $\mu$m) range after irradiation processing. The major products formed in these experiments include $CO_2$ (peak near 2340 $cm^{-1}$), $C_3O_2$ (2242 $cm^{-1}$), and $C_2O$ (1990 $cm^{-1}$; not shown in Fig. 4). Other, less abundant species such as $C_3O$, and $C_4O$ are also likely sources of the other, unidentified peaks shown in Fig. 4 (irradiation case).

The abundances of the major products are plotted against the total applied energy dose in Fig. 5 for both irradiation and photolysis experiments. Formation yields have been measured from the slopes of the linear parts of the curves and are listed in Table IV, along with yields calculated from other ice experiments described below. Since the intrinsic band strength of $C_2O$ is unknown, an estimate of its abundance was made assuming a value of $A = 1 \times 10^{-17}$ cm molecule$^{-1}$. Yields of $CO_2$ were

**TABLE IV**
**Yields, *G*, in Processing Experiments (in Units of Molecules per 100 eV Absorbed)**

| | $G$(CO) | | $G$($CO_2$) | | $G$($C_3O_2$) | |
|---|---|---|---|---|---|---|
| Initial ice | p+ | UV | p+ | UV | p+ | UV |
| CO | — | — | 0.25(4) | 0.9(2) | 0.24(4) | 0.014(1) |
| $CO_2$ | 1.1(1) | 8.1(3) | — | — | <0.001 | <0.001 |
| $C_3O_2$ | 0.68(4) | 1.1(1) | 0.12(2) | 0.074(4) | −4.3(4) | −6.5(4) |
| $H_2O + C_3O_2$ (10 : 1) | 0.063(8) | 0.045(5) | 0.019(4) | 0.13(1) | −0.13(1) | −0.47(9) |

*Note*. Numbers in parentheses represent uncertainty in final digit (e.g., "0.25(4)" = "0.25 ± 0.04"). Negative values indicate yields of destruction.

$0.25 \pm 0.04$ molecules per 100 eV absorbed for irradiation and $0.9 \pm 0.2$ for photolysis, differing by a factor of about 3.6. Briggs and Clay (1968) reported a value of $G(CO_2) = 0.24 \pm 0.01$ molecules per 100 eV for the gamma radiolysis of liquid CO at 77 K.

It is clear from Figs. 4 and 5 that $C_3O_2$ is much more effectively produced by irradiation than by photolysis. The measured $C_3O_2$ yields are $0.24 \pm 0.04$ for irradiation and $0.014 \pm 0.001$ for photolysis (differing by a factor of 17). This is the first time a significant difference has been reported in any direct comparison of these two processing techniques. The differences in both measurements of the $CO_2$ and $C_3O_2$ yields are most likely linked to the strength of the CO bond, whose dissociation energy is 11.1 eV. While 0.8-MeV protons may easily break this bond directly, e.g.,

$$CO \rightarrow C + O, \tag{2}$$

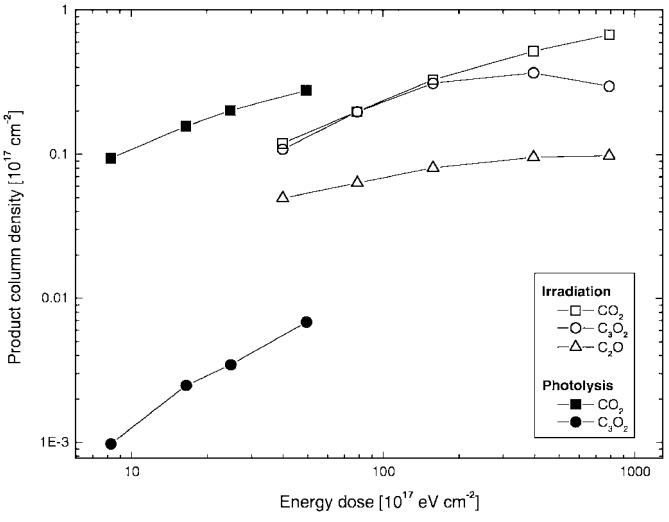


**FIG. 5.** Column density ($10^{17}$ cm$^{-2}$) versus energy dose ($10^{17}$ eV cm$^{-2}$) for the products of pure CO processing at 18 K by both proton irradiation (open symbols) and UV photolysis (filled symbols). Squares represent $CO_2$, circles $C_3O_2$, and triangles $C_2O$ (irradiation case only; $C_2O$ abundance assumes $A = 1 \times 10^{17}$ cm molecule$^{-1}$).

6 to 10 eV photons cannot.[3] Photolysis of CO proceeds through its indirect dissociation, a two-step process involving first the electronic excitation of one CO molecule (requires E > 8.4 eV) and its subsequent reaction with another to form $CO_2$ and a carbon atom,

$$CO \rightarrow CO^*, \tag{3}$$

$$CO^* + CO \rightarrow C + CO_2 \tag{4}$$

(Okabe 1978). Therefore, the formation of carbon chains and suboxides ($C_n$, $C_nO$, $C_nO_2$) is more effective in the irradiation case, whereas photolysis tends to form $CO_2$ before other carbon oxides.

$C_3O_2$ may also be a product to consider for $CO_2$ ice processing. In fact, $C_3O_2$ has been identified as a minor product in previous $CO_2$ processing studies with CO, $CO_3$, and $O_3$ in much higher abundances (e.g., Gerakines *et al.* 1996; Brucato *et al.* 1997). However, we find no indication of suboxide in the processed pure $CO_2$ ices studied here. Figure 6 contains IR spectra of the $CO_2$ ices in our processing experiments. Indeed, features due to CO (2139 cm$^{-1}$) and $CO_3$ (2046 cm$^{-1}$) appear strongly in our spectra (along with $O_3$ at 1045 cm$^{-1}$ and $CO_3$ at 1879 cm$^{-1}$; not shown in Fig. 6), but the $C_3O_2$ signal is not present. However, the feature of $C_2O$ is found at 1991 cm$^{-1}$ (although weak). We place upper limits on the $C_3O_2$ yields of $G < 0.001$ molecules (100 eV)$^{-1}$ in both irradiation and photolysis cases (Table IV), based on the noise levels in our laboratory spectra. Yields of CO were measured at $1.1 \pm 0.1$ molecules (100 eV)$^{-1}$ for irradiation and $8.1 \pm 0.3$ for photolysis (see Table IV). The origin of this difference in formation yields may be that the CO produced from the parent $CO_2$ molecules is more easily destroyed by the irradiation (as indicated in the pure CO experiments described previously) and thus displays a lower net yield of formation.

[3] While the end results will no doubt be quite different, the initiation of nitrogen chemistry in astrophysical ices should show a similar disparity between the processes of irradiation and photolysis, given that $N_2$, a molecule that is isoelectronic with CO, possesses a similarly high dissociation energy of 9.8 eV.

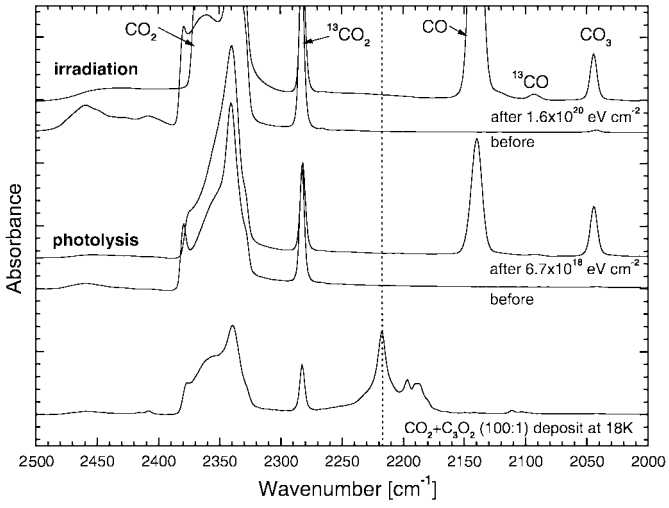


**FIG. 6.** Spectra of pure $CO_2$ from 2500 to 2000 $cm^{-1}$ (4 to 5 $\mu$m) before and after processing by proton irradiation (to a dose of $1.6 \times 10^{20}$ eV $cm^{-2}$) and UV photolysis (to a dose of $6.7 \times 10^{18}$ eV $cm^{-2}$). The spectrum of $CO_2 + C_3O_2$ (100 : 1) at 18 K (bottom) is shown for comparison. The dotted line indicates the peak position of the $C_3O_2$ stretching feature in the $CO_2 + C_3O_2$ (100 : 1) ice.

We have also studied the processing of pure $C_3O_2$ samples at 18 K. Spectra are given in Fig. 7. The major products observed in both irradiation and photolysis experiments were CO (at 2138 $cm^{-1}$), $CO_2$ (at 2345 $cm^{-1}$), $CO_3$ (at 2056 $cm^{-1}$), and $C_2O$ (at 1994 $cm^{-1}$). Other weaker features observed near 1948 and 1899 $cm^{-1}$ in the irradiation experiment are suggestive of longer carbon chains (e.g., Kurtz and Huffman 1990, Kranze *et al.* 1996). Yields measured in the irradiation experiment were $G(CO) = 0.68 \pm 0.04$, $G(CO_2) = 0.12 \pm 0.02$, and $G(-C_3O_2) = 4.3 \pm 0.4$. Yields in the photolysis experiment were $G(CO) = 1.1 \pm 0.1$, $G(CO_2) = 0.074 \pm 0.004$, and $G(-C_3O_2) = 6.5 \pm 0.4$. In each case, the suboxide destruction yield is much greater than the combined CO and $CO_2$ formation yields, suggesting the abundant formation of unidentified products such as $C_3O_2$ polymers.

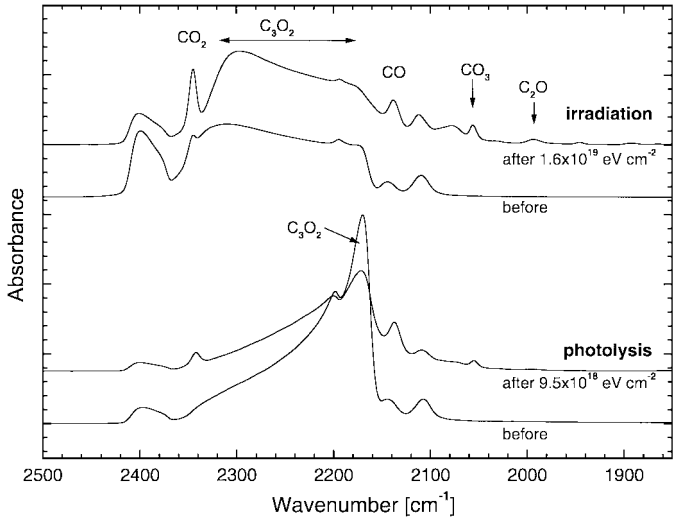


**FIG. 7.** Spectra of pure $C_3O_2$ at 18 K from 2500 to 1850 $cm^{-1}$ (4 to 5.4 $\mu$m) before and after processing by proton irradiation (thickness of 2.1 $\mu$m, irradiated to a dose of $1.6 \times 10^{19}$ eV $cm^{-2}$) and UV photolysis (thickness of 0.52 $\mu$m; photolyzed to a dose of $9.5 \times 10^{18}$ eV $cm^{-2}$).

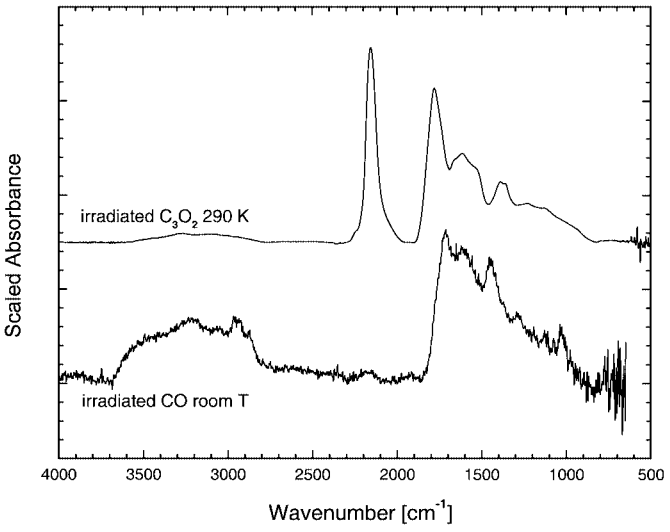


**FIG. 8.** Spectra of irradiated $C_3O_2$ warmed to 290 K (top) and irradiated CO after warming to room temperature (bottom).

CO and $CO_2$ are released during warming of the irradiated pure $C_3O_2$ sample. A residue remains at 290 K, and its spectrum is shown in Fig. 8. The spectrum of the room-temperature residue of irradiated CO, which was obtained with an FTIR microscope, is shown for comparison. The two spectra show some weak similarities, and the relative strengths of specific features vary from one to the other. The major peaks in the IR spectrum of the $C_3O_2$ residue (with possible functional group assignments based on their peak wavenumber) fall at 2156 (CO groups), 1781 (C═O bonds), 1617 (C═C bonds), and 1388/1361 $cm^{-1}$ (O═C–O groups). Weak absorption features also appear in the 3600–2850 $cm^{-1}$ region, indicative of cyclic carbon structures; these features may imply the presence of $C_3O_2$ thermal polymer, as its structure is likely a polycyclic unsaturated lactone as described in Kybett *et al.* (1965) and the references therein. The residue of irradiated CO has a much weaker feature near 2160 $cm^{-1}$, and strong peaks at 1712, 1614, 1449, 1288, and 1031 $cm^{-1}$. Absorptions in the 3600–2850 $cm^{-1}$ region are much stronger in this case. The color of the CO residue is dark reddish brown, and further characterizations in the UV and visible wavelength regions are in progress.

Since the ice environments of comets and interstellar ices are typically thought to be $H_2O$-dominated, the formation and destruction of $C_3O_2$ should be considered in ice samples where CO, $CO_2$, and $C_3O_2$ have been diluted in $H_2O$. Work already present in the literature has shown that the major products of $H_2O + CO$ processing are $CO_2$, HCO, $H_2CO$, and $CH_3OH$ (photolysis: Sandford *et al.* 1988; irradiation: Hudson and Moore 1999). No detection of $C_3O_2$ has been noted. Previous studies

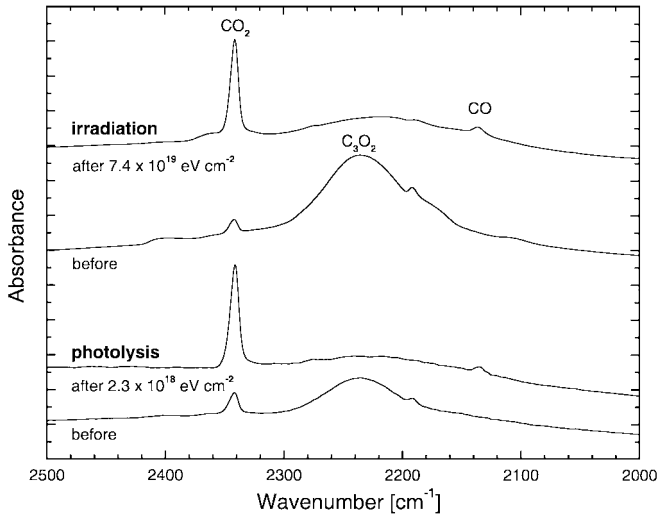


**FIG. 9.** Spectra of $H_2O + C_3O_2$ (10 : 1) at 18 K from 2500 to 2000 $cm^{-1}$ (4 to 5 $\mu$m) before and after processing by proton irradiation (to a dose of $7.4 \times 10^{19}$ eV $cm^{-2}$) and UV photolysis (to a dose of $2.3 \times 10^{18}$ eV $cm^{-2}$).

of $H_2O + CO_2$ ices have shown that the major products of processing are CO, HCO, and $H_2CO_3$ (photolysis and irradiation: Gerakines *et al.* 2000), and, again, no detection of $C_3O_2$ was noted.

We have studied the processing of $H_2O + C_3O_2$ ice at low temperature. The $H_2O + C_3O_2$ (10 : 1) ice sample's spectrum before and after processing is shown in Fig. 9. The two major products of both irradiation and photolysis were found to be CO and $CO_2$. Product column densities in the sample are shown in Fig. 10 as a function of absorbed energy dose. In the irradiation experiment, these species initially formed with yields of $G(CO) = 0.063 \pm 0.008$ and $G(CO_2) = 0.019 \pm 0.004$ (to a dose of $3 \times 10^{19}$ eV $cm^{-2}$, see Fig. 10). Yields dropped at higher doses. The $C_3O_2$ was destroyed by irradiation with a destruction yield of $G(-C_3O_2) = 0.13 \pm 0.01$ to a dose of $3 \times 10^{19}$ eV $cm^{-2}$. In the photolysis experiment, where the total energy dose was $2.4 \times 10^{18}$ eV $cm^{-2}$, only linear production and destruction rates were apparent, and we measured yields of $G(CO_2) = 0.13 \pm 0.01$, $G(CO) = 0.045 \pm 0.005$, and $G(-C_3O_2) = 0.47 \pm 0.09$ (see Fig. 10).

## 4. DISCUSSION AND IMPLICATIONS

We have found that $C_3O_2$ has a mid-IR spectrum that is sensitive to the effects of dilution in a molecular matrix. The differences in the $\nu_3$ peak's position between different ice matrices at low temperature are quite large. The extreme values of the peak position for the $\nu_3$ $C_3O_2$ features are 2253 $cm^{-1}$ in an $N_2$-dominated ice at 18 K and 2178 $cm^{-1}$ in a pure $C_3O_2$ ice at 18 K, with values for ices dominated by CO, $CO_2$, and $H_2O$ falling in between. The width of the $\nu_3$ feature also varies greatly, from only 8 $cm^{-1}$ in a CO-dominated ice at 18 K to 90 $cm^{-1}$ in one that is $H_2O$-dominated as 18 K. Hence, the detection of this absorption feature in either the ISM or in planetary ices could lead to highly accurate determinations of the overall ice environment.

However, solid-phase $C_3O_2$ has not been positively identified in recent mid-infrared observations conducted by the Infrared Space Observatory (ISO). Figure 11 compares two ISO short-wavelength spectrometer (SWS) observations of high-mass protostars, W33A and NGC 7538 IRS9, to laboratory spectra of $H_2O + C_3O_2$ (10 : 1) and $CO + C_3O_2$ (100 : 1) at 18 K. Although small features do seem to exist in the spectral region near the expected position of the $C_3O_2$ $\nu_3$ feature, these are likely well within the noise of the observed data. The observations of W33A

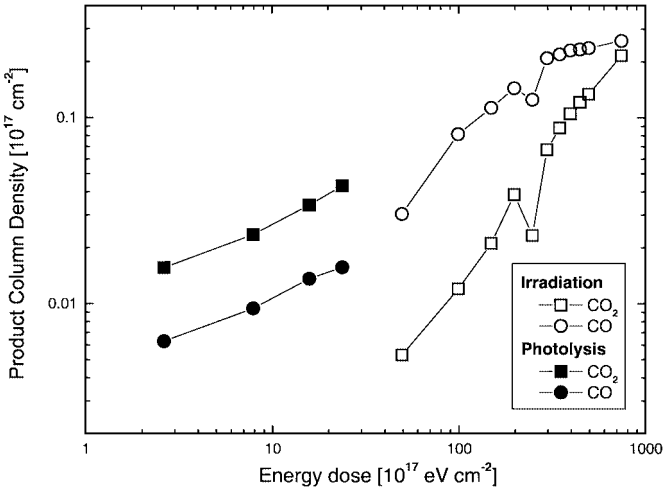


**FIG. 10.** Column density ($10^{17}$ $cm^{-2}$) versus energy dose ($10^{17}$ eV $cm^{-2}$) for the products of $H_2O + C_3O_2$ (10 : 1) ice processing at 18 K by both proton irradiation (open symbols) and UV photolysis (filled symbols). Squares represent $CO_2$, and circles CO.

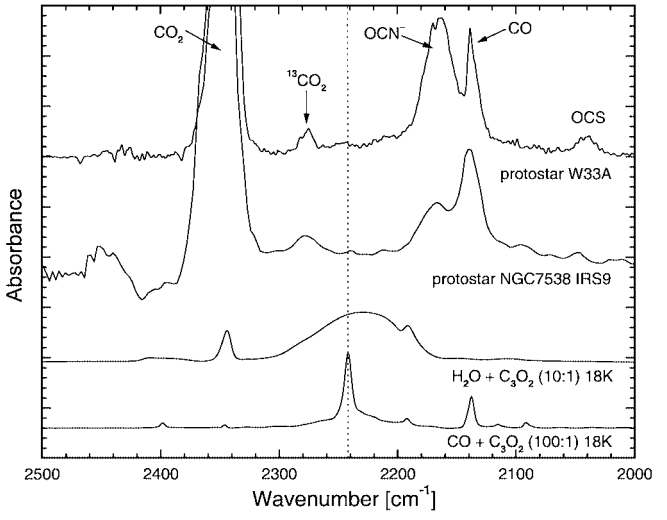


**FIG. 11.** ISO-SWS spectra of the protostars W33A (Gibb *et al.* 2000) and NGC 7538 IRS9 (Whittet *et al.* 1996) in the region of the $C_3O_2$ $\nu_3$ stretching feature. The dotted line indicates the position (2242 $cm^{-1}$) of the $C_3O_2$ $\nu_3$ stretching feature in the $CO + C_3O_2$ (100 : 1) ice sample.

(Gibb *et al*. 2000) were made at a spectral resolution of $\lambda/\Delta\lambda = 1500$, while those of NGC 7538 IRS9 (Whittet *et al*. 1996) have a lower resolution of $\lambda/\Delta\lambda = 500$. Upper limits on the $C_3O_2$ column density in these observations, based on the level of the noise between 2220 and 2250 $cm^{-1}$, are about $5 \times 10^{15}$ $cm^{-2}$ for W33A (0.05% of $H_2O$) and $1 \times 10^{15}$ $cm^{-2}$ for NGC 7538 IRS9; 0.01% $H_2O$; $H_2O$ column densities in these lines of sight may be found in Gibb *et al*. (2000). Other molecules such as $N_2O$ also have absorption features in the 2200–2300 $cm^{-1}$ region, and, if present, would lower this limit even further ($N_2O$ has an absorption that falls at about 2235 $cm^{-1}$; see e.g., Elsila *et al*. 1997). This dearth of $C_3O_2$ comes despite the relatively high abundance of solid CO and $CO_2$ present in the sampled protostellar environments: the total amount of solid CO ranges from 2 to 15% of the $H_2O$ ice column density (Gibb *et al*. 2000), and $CO_2$ from about 12 to 22% (Gerakines *et al*. 1999). Most other ice components are found at the 1% level relative to $H_2O$.

We have shown that $C_3O_2$ forms efficiently in pure CO ice samples when processed by irradiation with a yield of about 0.25 molecules per 100 eV absorbed. The yield of $C_3O_2$ by photolysis in similarly prepared CO ices is about 20 times smaller. However, it is not formed in significant abundances from pure $CO_2$ ice or from mixtures dominated by $H_2O$. Since interstellar ices toward massive protostars are largely composed of $H_2O + CO_2 + CH_3OH$ in the ratio of approximately 100 : 20 : 10 (Gerakines *et al*. 1999; Dartois *et al*. 1999; Gibb *et al*. 2000), it may not be surprising to note that $C_3O_2$ is not found there.

This may not be the final verdict for interstellar solid $C_3O_2$, however, since an important observational bias exists in the ISO dataset because of the sensitivity limits of its instruments. The majority of sources observed were highly constrained to those bright in the mid infrared and, in the case of ice detections, almost entirely high-mass protostars. Detailed observations of a more varied set of sight lines, including those toward background field stars as well as lower mass embedded protostars, may yet yield a detection of interstellar $C_3O_2$, as, among other factors, the fraction of CO in the nonpolar ($H_2O$-poor) ice phase is higher in these colder environments (e.g., Chiar *et al*. 1995). Unfortunately, ISO observations toward the background field star Elias 16, which focused on detections of solid CO and $CO_2$ (Whittet *et. al*. 1998), omitted the wavelength region containing the $C_3O_2$ $\nu_3$ stretch because of time constraints imposed by the low flux level of this source.

There are also no positive detections of $C_3O_2$ toward comets (see, e.g., Irvine *et al*. 2000). This may be due to the fact that gas-phase $C_3O_2$ easily dissociates in the environment of cometary comae, as described in detail in Huntress *et al*. (1991). There is, however, reason to believe that comets may provide an environment capable of producing $C_3O_2$. Comets contain large amounts of CO as a parent volatile in their nuclei, as evidenced by observations of the gases released in their comae (e.g., Irvine *et al*. 2000). This is not surprising, since comets are thought to have formed out of interstellar ices (either directly or indirectly) as the natal cloud condensed to form the young Sun. Highly volatile molecules such as CO may even be physically separated from $H_2O$ in the nuclei of short-period comets by heating and recooling during successive perihelion passages, resulting in a type of "cryogenic distillation." The processing of such purer cometary CO ices by solar UV or galactic cosmic rays may lead to $C_3O_2$ in higher abundances than may be found in the interstellar medium. Based on our experiments, it is also likely that cometary $C_3O_2$ produced from energetic processing would remain intact in the nuclear ice or be converted by energetic processing to a dark polymeric residue. The large increase in the $C_3O_2$ vapor pressure from 110 to 125 K would imply that the release of $C_3O_2$ would increase greatly as the comet approached the Sun from a distance of about 7 to 5 AU. This increase in $C_3O_2$ would manifest itself as an increase in the amount of CO emission in the comet's coma and the growth of an extended source of CO as the gas-phase $C_3O_2$ is dissociated. Of course, few comets are observed at such heliocentric distances because they are extremely faint, but emerging technologies, such as infrared interferometry or spaced-based telescopes, could make such observations possible.

## APPENDIX: A COMMENT ABOUT THE REPORTING OF PRODUCT YIELDS

In this paper, we have presented initial formation and destruction yields for the products and reactants in our processing experiements. This is generally not the standard way of reporting radiolysis experiements, where a yield is reported after the application of a specified dose. For example, one might report that a certain number of molecules of product were created after a dose 100 eV, or that product's yield, or "*G* value." If a higher dose is applied, it is possible that the value of *G* reported (the number of products divided by total dose applied) will drop, as it represents the *yield averaged over the course of the entire irradiation*. This would most likely be due to the fact that the number of reactants is dropping while the number of products is rising, and the sample is approaching some sort of equilibrium chemistry (after which the reactant and product abundances remain constant). Such an example is shown in Fig. 5, where the average yield of $C_3O_2$ from CO is initially constant (as shown by the linear growth for doses less than about $2 \times 10^{19}$ eV $cm^{-2}$) and later drops as the energy dose is further increased.

We have not reported the equilibrium constants here or the average formation rates of products but rather the rates of formation given by the zeroth- or first-order chemical reaction kinetics that take place when the energy applied interacts with the reactant molecules. This happens to be the standard way in which UV photolysis results are reported; see, e.g., Gerakines *et al*. (1996). UV formation and destruction rates are generally given in terms of cross sections as opposed to yields, but the two parameters provide the same information about the reactions and may be directly compared by a reasonably simple transformation of units (see discussion in Gerakines *et al*. 2000).

Initial formation rates, as opposed to the equilibrium rates, are given priority here because it is rare in an astrophysical context, given the typically small number of interactions per molecule or per unit time, to find a system *actually in chemical equilibrium*. Moreover, the simple mixtures we are studying (we have included only one or two components) do not by any means represent the complex ices found in space, but are merely models for the behavior of certain astrophysical ice components. It is therefore more appropriate here to study the low-order reaction kinetics, as they may be more easily implemented in chemcial models where many more components may be included.

## ACKNOWLEDGMENTS

We gratefully thank Reggie Hudson for a myriad of helpful discussions and good ideas. Steve Brown, Scott Kniffin and Claude Smith from NASA/GSFC's Radiation Effects Facility are thanked for help with the irradiations. Alex Montoya from NASA/GSFC's Materials Engineering Branch is thanked for

use of the FTIR microscope. This work was performed while P.A.G. held a NRC-NAS/NASA-GSFC research associateship.

## REFERENCES

Ames, L. L., D. White, and D. E. Mann 1963. Infrared absorption spectra of carbon suboxide and malononitrile in solid argon matrices. *J. Chem. Phys.* **38**, 910–917.

Briggs, J. P., and P. G. Clay 1968. Formation of polymeric carbon suboxide during gamma radiolysis of liquid carbon monoxide at 77°K. *Nature* **218**, 355.

Brodie, B. C. 1873. Note on the synthesis of marsh-gas and formic acid, and on the electric decomposition of carbonic oxide. *Proc. Roy. Soc. London* **21**, 245–247.

Brucato, J. R., M. E. Palumbo, and G. Strazzulla 1997. Carbonic acid by ion implantation in water/carbon dioxide ice mixtures. *Icarus* **125**, 135–144.

Chiar, J. E., A. J. Adamson, T. H. Kerr, and D. C. B. Whittet 1995. High-resolution studies of solid CO in the Taurus dark cloud: Characterizing the ices in quiescent clouds. *Astrophys. J.* **455**, 234–243.

Dartois, E., W. Schutte, T. R. Geballe, K. Demyk, P. Ehrenfreund, and L. d'Hendecourt 1999. Methanol: The second most abundant ice species towards the high-mass protostars RAFGL7009S and W 33A. *Astron. Astrophys.* **342**, L32–L35.

Eberhardt, P., D. Krankowsky, W. Schulte, P. Lämmerzahl, J. J. Berthelier, J. Woweries, U. Stubbemann, R. R. Hodges, J. H. Hoffman, and J. M. Illiano 1987. The CO and $N_2$ abundance in Comet P/Halley. *Astron. Astrophys.* **187**, 481–484.

Elsila, J., L. J. Allamandola, and S. A. Sandford 1997. The 2140 $cm^{-1}$ (4.673 $\mu$m) solid CO band: The case for interstellar $O_2$ and $N_2$ and the photochemistry of nonpolar interstellar ice analogs. *Astrophys. J.* **479**, 818–838.

Ewing, G. E., and G. C. Pimentel 1961. Infrared spectrum of solid carbon monoxide. *J. Chem. Phys.* **35**, 925–930.

Festou, M. C., P. D. Feldman, M. F. A'Hearn, C. Arpigny, C. B. Cosmovici, A. C. Danks, L. A. McFadden, R. Gilmozzi, P. Patriarchi, G. P. Tozzi, M. K. Wallis, and H. A. Weaver 1986. IUE observations of Comet Halley during the VEGA and Giotto encounters. *Nature* **321**, 361–368.

Gerakines, P. A., W. A. Schutte, J. M. Greenberg, and E. F. van Dishoeck 1995. The infrared band strengths of $H_2O$, CO, and $CO_2$ in laboratory simulations of astrophysical ice mixtures. *Astron. Astrophys.* **296**, 810–818.

Gerakines, P. A., W. A. Schutte, and P. Ehrenfreund 1996. Ultraviolet processing of interstellar ice analogs. I. Pure ices. *Astron. Astrophys.* **312**, 289–305.

Gerakines, P. A., D. C. B. Whittet, P. Ehrenfreund, A. C. A. Boogert, A. G. G. M. Tielens, W. A. Schutte, J. E. Chiar, E. F. van Dishoeck, T. Prusti, F. P. Helmich, and Th. de Graauw 1999. Observations of solid carbon dioxide in molecular clouds with the Infrared Space Observatory. *Astrophys. J.* **522**, 357–377.

Gerakines, P. A., M. H. Moore, and R. L. Hudson 2000. Carbonic acid production in $H_2O + CO_2$ ices—UV photolysis vs. proton bombardment. *Astron. Astrophys.* **357**, 793–800.

Gibb, E. L., D. C. B. Whittet, W. A. Schutte, A. C. A. Boogert, J. E. Chiar, P. Ehrenfreund, P. A. Gerakines, J. V. Keane, A. G. G. M. Tielens, E. F. van Dishoeck, and O. Kerkhof 2000. An inventory of intersteller ices toward the embedded protostar W33A. *Astrophys. J.* **536**, 347–356.

Hagen, W., A. G. G. M. Tielens, and J. M. Greenberg 1983. A laboratory study of the infrared spectra of interstellar ices. *Astron. Astrophys. Suppl. Ser.* **51**, 389–416.

Haring, R. A., R. Pedrys, D. J. Oostra, A. Haring, and A. E. de Vries 1984. Reactive sputtering of simple condensed gases by keV ions. II Mass spectra. *Nucl. Instrum. Methods. Phys. Res.* ***B*** **5**, 476–482.

Hudson, R. L., and M. H. Moore 1995. Far-IR spectral changes accompanying proton irradiation of solids of astrochemical interest. *Radiat. Phys. Chem.* **45**, 779–789.

Hudson, R. L., and M. H. Moore 1999. Laboratory studies of the formation of methanol and other organic molecules by water + carbon monoxide radiolysis: relevance to comets, icy satellites, and interstellar ices. *Icarus* **140**, 451–461.

Huntress, W. T. Jr., M. Allen, and M. Delitsky 1991. Carbon suboxide in Comet Halley? *Nature* **352**, 316–318.

Irvine, W. M., F. P. Schloerb, J. Crovisier, B. Fegley Jr., and M. J. Mumma 2000. Comets: A link between interstellar and nebular chemistry. In *Protostars and Planets IV* (V. Mannings, A. P. Boss, and S. S. Russell, Eds.), pp. 1159–1200. Univ. of Arizona Press, Tucson.

Jiang, G. J., W. B. Person, and K. G. Brown 1975. Absolute infrared intensities and band shapes in pure solid CO and CO in some solid matrices. *J. Chem. Phys.* **64**, 1201–1211.

Kouchi, A. 1987. Vapour pressure of amorphous $H_2O$ ice and its astrophysical implications. *Nature* **330**, 550–552.

Kranze, R. H., C. M. L. Rittby, and W. R. M. Graham 1996. Fourier transform infrared and theoretical isotopic study of the $\nu_4(\sigma_u)$ and $\nu_5(\sigma_u)$ modes of linear $C_7$. *J. Chem. Phys.* **105**, 5313–5320.

Kuiper, G. P. 1957. The atmosphere and the cloud layer of Venus. In *The Threshold of Space* (M. Zelikoff, Ed.), pp. 85–86. Pergamon Press, New York.

Kurtz, J., and D. R. Huffman 1990. Combined infrared and ultraviolet–visible spectroscopy of matrix–isolated carbon vapor. *J. Chem. Phys.* **92**, 30–35.

Kybett, B. D., G. K. Johnson, C. K. Barker, and J. L. Margrave 1965. The heats of formatoin and polymerization of carbon suboxide. *J. Phys. Chem.* **69**, 3603–3606.

Lind, S. C. 1928. *The Chemical Effects of Alpha Particles and Electrons*. Chemical Catalog Co, New York.

McDougall, L. A., and J. E. Kilpatrick 1965. Entropy and related thermodynamic properties of carbon suboxide. *J. Chem. Phys.* **42**, 2311–2321.

Miller, F. A., and W. G. Fateley 1964. The infrared spectrum of carbon suboxide. *Spectrochim. Acta* **20**, 253–266.

Okabe, H. 1978. *Photochemistry of Small Molecules*. Wiley, New York.

Pipes, J. G., J. A. Roux, A. M. Smith, and H. E. Scott 1978. Infrared transmission of contaminated cryocooled optical windows. *AIAA J.* **16**, 984–990.

Plummer, W. T., and R. K. Carson 1970. Venus clouds: Test for carbon suboxide. *Astrophys. J.* **159**, 159–163.

Sagdeev, R. Z., and 37 colleagues 1986. Television observations of Comet Halley from VEGA spacecraft. *Nature* **321**, 262–266.

Sandford, S. A., L. J. Allamandola, A. G. G. M. Tielens, and G. J. Valero 1988. Laboratory studies of the infrared spectral properties of CO in astrophysical ices. *Astrophys. J.* **329**, 498–510.

Smith, W. H., and G. E. Leroi 1966. Infrared and Raman spectra of carbon suboxide in condensed phases. *J. Chem. Phys.* **45**, 1767–1777.

Sugimoto, S., M. Nishii, and T. Sugiura 1986. Radiation-induced chemical reactions of carbon monoxide and hydrogen mixture. 3. Solid materials produced under irradiation. *Radiat. Phys. Chem.* **27**, 147–151.

Whittet, D. C. B., W. A. Schutte, A. G. G. M. Tielens, A. C. A. Boogert, Th. de Graauw, P. Ehrenfreund, P. A. Gerakines, F. P. Helmich, T. Prusti, and E. F. van Dishoeck 1996. An ISO-SWS view of interstellar ices: First results. *Astron. Astrophys.* **315**, L357–L360.

Whittet, D. C. B., P. A. Gerakines, A. G. G. M. Tielens, A. J. Adamson, A. C. A. Boogert, J. E. Chiar, Th. de Graauw, P. Ehrenfreund, T. Prusti, W. A. Schutte, B. Vandenbussche, and E. F. van Dishoeck 1998. Detection of abundant $CO_2$ ice in the quiescent dark cloud medium toward Elias 16. *Astrophys. J.* **498**, L159–L163.

Woods, T. N., P. D. Feldman, and K. F. Dymond 1987. The atomic carbon distribution in the coma of Comet P/Halley. *Astron. Astrophys.* **187**, 380–384.